Inversion for atmosphere duct parameters using real radar sea clutter*

Sheng Zheng(盛 峥)[a)b)] and Fang Han-Xian(方涵先)[a)†]

[a)] *Institute of Meteorology, PLA University of Science and Technology, Nanjing* 211101, *China*
[b)] *Sate Key Laboratory of Space Weather, Chinese Academy of Sciences, Beijing* 100190, *China*

(Received 25 June 2011; revised manuscript received 19 September 2011)

This paper addresses the problem of estimating the lower atmospheric refractivity (M profile) under nonstandard propagation conditions frequently encountered in low altitude maritime radar applications. The vertical structure of the refractive environment is modeled using five parameters and the horizontal structure is modeled using five parameters. The refractivity model is implemented with and without a priori constraint on the duct strength as might be derived from soundings or numerical weather-prediction models. An electromagnetic propagation model maps the refractivity structure into a replica field. Replica fields are compared with the observed clutter using a squared-error objective function. A global search for the 10 environmental parameters is performed using genetic algorithms. The inversion algorithm is implemented on the basis of S-band radar sea-clutter data from Wallops Island, Virginia (SPANDAR). Reference data are from range-dependent refractivity profiles obtained with a helicopter. The inversion is assessed (i) by comparing the propagation predicted from the radar-inferred refractivity profiles with that from the helicopter profiles, (ii) by comparing the refractivity parameters from the helicopter soundings with those estimated. This technique could provide near-real-time estimation of ducting effects.

Keywords: atmosphere duct, radar clutter, refractivity from clutter, genetic algorithm

PACS: 93.85.Ly, 41.20.Jb **DOI:** 10.1088/1674-1056/21/2/029301

1. Introduction

Surface-based ducts appear about 15% of the time worldwide, 25% of the time off Southern California Coast and 50% of the time in the Persian Gulf.[1] Many efforts in remote sensing and numerical weather prediction have been made to better estimate the refractivity structure in the lowest 1000 m above the sea surface. In order to estimate electromagnetic wave propagation in the atmospheric environment, analyse ducts and their influence on the electric systems, the research on atmosphere duct attracts more and more attention from some institutions and military organizations. Because the effects of surface-based ducting are visibly manifested in radar clutter, it might be feasible to extract information about the duct refractive structure from the clutter. Such a "refractivity-from-clutter" (RFC) capability might provide near-real-time, azimuth-dependent information about the ducting conditions. Inferring refractivity parameters from observations of radar clutter is an inverse problem. On account of the complexity of parabolic equation and the ill-posed refractivity parameter inversion, the technique of RFC confronts too many difficulties. Therefore, seeking a high efficiency and steady inverse algorithm is essential to solve the problem.

RFC techniques estimate the modified refractivity profile (M profile) by taking advantage of the changes in radar clutter return due to atmospheric refraction.[2−15] Detailed discussion about these different RFC algorithms can be found in Refs. [8] and [9].

In this paper, the inversion algorithm is implemented on real radar sea clutter from Wallops Island, Virginia. Reference data are from range-dependent refractivity profiles obtained with a helicopter. The retrieved values demonstrate the feasibility of this approach to estimating the environmental refractive structure from radar data itself.

*Project supported by the National Natural Science Foundation of China (Grant No. 41105013), the Natural Science Foundation of Jiangsu Province, China (Grant No. BK2011122), and the Specialized Research Fund for State Key Laboratories, China (Grant No. 201120FSIC-03).

†Corresponding author. E-mail: 19994035@sina.com

© 2012 Chinese Physical Society and IOP Publishing Ltd

2. Forward modeling and inversion algorithm

2.1. Environmental and propagation model

Ten-parameter refractivity model has been proposed by Naval Force Physics Laboratory in California, which can be described as

$$\boldsymbol{m} = (\delta, c_1, z_\mathrm{b}, z_\mathrm{thick}, M_\mathrm{d}, Zb_1, Zb_2, Zb_3, Zb_4, Zb_5)^\mathrm{T}. \tag{1}$$

The vertical structure of the refractive environment is modeled using the first five parameters and the horizontal structure is modeled using the last five parameters. Here δ is the evaporation duct height, c_1 is the slope in the mixed layer, z_b is the trapping-layer base height, z_thick is the thickness of the inversion layer and M_d is M deficit of the inversion layer, Zb_1–Zb_5 is base height coefficient 1–coefficient 5. The value of modified refractivity as a function of height z is given by

$$M(z) = M_0 + \begin{cases} M_1 + c_0\left(z - \delta \log \dfrac{z}{z_0}\right), & \text{for } z < z_\mathrm{d}, \\ c_1 z, & \text{for } z_\mathrm{d} < z < z_\mathrm{b}, \\ c_1 z_\mathrm{b} - M_\mathrm{d}\dfrac{z - z_\mathrm{b}}{z_\mathrm{thick}}, & \text{for } z_\mathrm{b} < z < z_\mathrm{t}, \\ c_1 z_\mathrm{b} - M_\mathrm{d} + c_2(z - z_\mathrm{t}), & \text{for } z_\mathrm{t} < z. \end{cases} \tag{2}$$

The base-height coefficients were each determined as plus/minus a fraction of the square root of the corresponding eigenvalue. The principal components are determined using the Karhunen–Loeve method. First, 10^6 Markov realizations of base height variation versus range were generated. For each kilometer, the base height was updated using a Gaussian distribution with a standard deviation of 1 m (this is arbitrarily chosen since the process is linear and it can be scaled later). Due to the transition from land to sea, the profiles were referenced at 10 km so that they all had a value of 0 at range 10 km. Next, the main eigenvectors and eigenvalues were determined from the correlation matrix generated from the realizations of the base height. For the environmental model, the weighting for each eigenvector is picked from a uniform distribution between plus/minus the square root of the eigenvalues. This effectively constrains the base height variations to ±50 m over the range of 0 to 100 km, but allows substantial freedom within that range.

In practical implementations, prior information that might be available from a variety of sources (e.g., numerical weather prediction models, atmospheric soundings, etc.) could improve the quality of the inverse problem solutions. The boundary of refractivity parameters is shown in Table 1 (The reader may refer to Ref. [4] for the detailed description).

Table 1. Parameter search bounds for ten-parameter model.

Parameter	Lower bound	Upper bound
Thickness/m	0	100
M-deficit/M-units	0	100
Mixed layer slope M-units/m	–1	0.4
Evaporation duct height/m	0	40
Base height/m	3	300
Base height coefficient 1	–570	570
Base height coefficient 2	–190	190
Base height coefficient 3	–110	110
Base height coefficient 4	–80	80
Base height coefficient 5	–65	65

The most commonly used approach to modeling the wave propagation in the troposphere is the Fourier split-step solution to the parabolic equation. This numerical solution is a forward solver with the ability to handle vertical and horizontal inhomogeneities in the refractive profile and is capable of performing accurate propagation loss estimation in complicated environments.

2.2. Inversion algorithm

It is assumed that the difference (dB) between the observed $\boldsymbol{P}_\mathrm{c}^\mathrm{obs}$ and modeled $\boldsymbol{P}_\mathrm{c}(\boldsymbol{m})$ clutter is Gaussian. This leads to a simple least squares objective function

$$\phi(\boldsymbol{m}) = \boldsymbol{e}^\mathrm{T}\boldsymbol{e}, \tag{3}$$

where $\boldsymbol{e} = \boldsymbol{P}_\mathrm{c}^\mathrm{obs} - \boldsymbol{P}_\mathrm{c}(\boldsymbol{m})$.

The genetic algorithm code [Gerstoft *et al.*, 2000] is used to optimize Eq. (3). The genetic algorithms (GA)-search parameters were: parameter quantization 128 values; population size 64; reproduction size 0.5; cross-over probability 0.05; number of iterations for each population 2000; number of populations 10. Thus 2×10^4 forward modeling runs were performed for each inversion. For further information about the use of GA for parameter estimation, see Gerstoft [2003].

3. Radar model and cross section

3.1. Radar model

The received power $P_{\rm c}$ from radar sea clutter could be calculated by

$$P_{\rm c} = \frac{4\pi P_{\rm t} G_{\rm t} G_{\rm r} A_{\rm c} \sigma^o}{L^2 \lambda^2}, \tag{4}$$

where $P_{\rm t}$ is the transmitted power, $G_{\rm t}$ and $G_{\rm r}$ are the respective transmit and receiving antenna gains, λ is the wavelength, $A_{\rm c}$ is the illuminated area and σ^0 is the sea clutter normalized radar cross section. At low grazing angles, $A_{\rm c}$ is a linear function of range r, thus equation (3) can be rewritten as

$$P_{\rm c} = \frac{C\sigma^o r}{L^2}, \tag{5}$$

where C accounts for all of the constant terms in Eq. (3). Letting the symbols $P_{\rm c}$, C, σ^0, and L represent the associated values in dB as opposed to real numbers, the received signal power from the clutter can be modeled as follows:

$$P_{\rm c} = -2L + 10\log_{10}(r) + \sigma^o + C. \tag{6}$$

Here, some stochastic variations in range as a Markov process are simulated as noise.

3.2. Radar cross section

Assumptions about the radar cross section are essential for the RFC inversions, especially the range and grazing angle dependency. Despite the considerable progress in low angle backscatter modeling,[16–18] this ability is used only indirectly as it complicates the inversion considerably. The outputs of linked weather, wave, clutter and propagation models may eventually be brought into the refractivity inversion algorithms. However, assessing the goodness of the linked models should precede that step and such investigations are only beginning.

For vertical polarization there is still some question whether the grazing angle dependence is φ^0, φ^4 or some value in between. For inferring evaporation duct heights from radar sea echo, Rogers *et al.*[2] found that while their data did not provide a definitive answer to the grazing angle dependency, the use of $\sigma \propto \varphi^0$ in the duct height estimation algorithm generated better results. This model is chosen here.

4. Inversion of SPANDAR data

4.1. Radar and reference data

A polar plot of S/N (or clutter map) at 0^0 elevation from a ducting event is shown in Fig. 1 that occurred in April 1998.

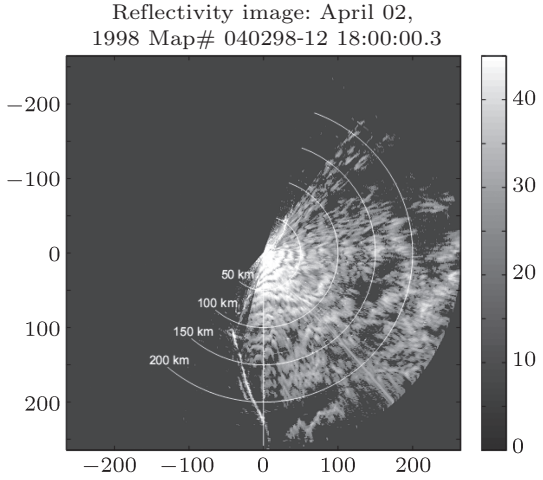


Fig. 1. Reflectivity map (dBZ) from SPANDAR, the elevation angle is 0° and horizontal and vertical ranges are in kilometer.

Radar data were obtained using the Space Range Radar (SPANDAR). The radar system parameters as configured for the data taken here are shown in Table 2.

Table 2. Space range radar parameters.

Parameter	Measurement
Frequency/GHz	2.84
Power/dB	91.40
Beamwidth/(°)	0.39
Antenna gain/dB	52.80
Height/m	30.78
Polarization	vertical
Range bin width/m	600

Meteorological soundings were obtained by an instrumented helicopter which would fly in and out on the 150° radial from a point 4 km due east of the SPANDAR, is shown in Fig. 2.

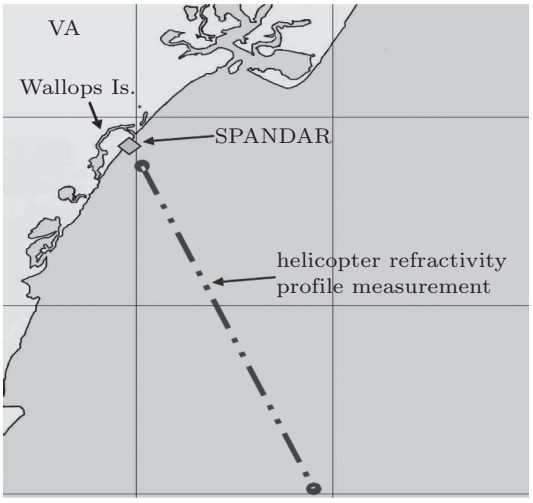


Fig. 2. Wallops '98 Experiment: SPANDAR radar and the helicopter measurements (37.83 °N, 75.48 °W).

4.2. Experiments result without meteorology constraints

Figure 3 summarizes the inversion and the assessment of the inversion results for a single frame. First, the clutter $\boldsymbol{P}_{\rm c}^{\rm obs}$ along azimuth 150° and 10 km–60 km in range is extracted from the clutter map (Fig. 1) and shown as a solid line in Fig. 3(a). Clutter-return intensifications are seen at around 25, 35, and 45 km. Optimizing the fit between the replica $\boldsymbol{P}_{\rm c}(\boldsymbol{m})$ and the observed data with respect to the environmental parameters in Table 2 was carried out. The best matching replica is shown as dash dotted line and for reference, the modeled clutter returns from the helicopter profiles are shown as solid line. The objective function, Eq. (3), is concerned only with minimizing the error and only indirectly is there optimization for the location and the number of peaks. The inversion can visually be judged by examining how the peaks in the replica are matched.

The second plot (Fig. 3(b)) shows the estimated refractivity profiles (dash dotted) along with the helicopter refractivity profiles (solid line). Because this is an undetermined problem, the best fit might not correspond to the true profile. An equivalent profile that gives the best match to the clutter return is obtained. The next two plots show the modeled propagation loss for the optimal environment and the helicopter profiles, respectively. The difference of these two (bottom plot) gives an indication of how well the inverted profile is able to predict the propagation loss.

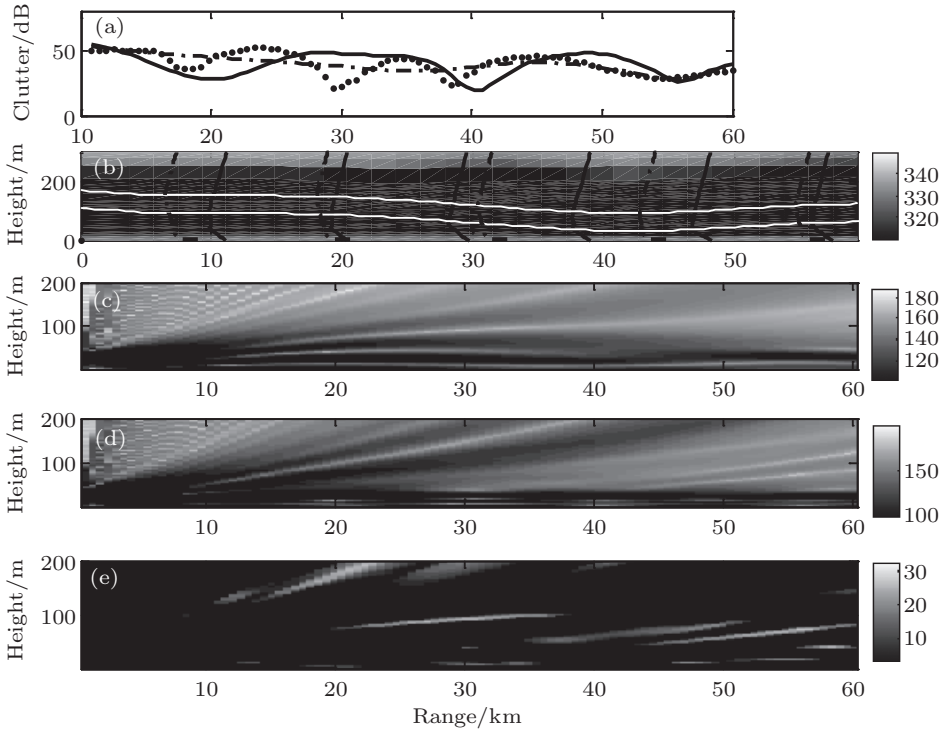


Fig. 3. Inversions based on the clutter return shown in Fig. 2 along azimuth 150° without meteorology constraints: (a) the clutter return (dB) as observed by the radar data (dotted), the modeled return using the retrieval profile (dash dotted) and modeled return from the observed profile (solid line); (b) observed profiles measured from helicopter (solid line) and inverted profiles (dash dotted); (c) coverage diagram (dB) corresponding to the inverted profiles; (d) coverage diagram (dB) based on helicopter profiles; (e) difference (dB) between coverage diagrams Figs. 3(c) and 3(d).

5. Inversion with meteorology constraints

5.1. Meteorology constraint equation

Considering that a sounding is available from which we can diagnose the top of the trapping layer ($z_{\rm top}^{\rm obs}$) and its associated value of modified refractivity. For a surface duct, this will correspond to the minimum value of the M profile. Assuming that the value of modified refractivity immediately above the sea surface remains constant, that the air mass above the top of the trapping layer remains constant in time and that the lapse-rate for refractivity in that air mass is the same, which leads to the relationship for any value of $z_{\rm top}$. $c_{\rm lap}$ is taken as either the slope for a convective boundary layer ($c_1 = 0.118$ M units/m) or average slope above the trapping layer ($c_2 = 0.118$ M units/m). The refractivity inversion algorithm tends to overestimate the degree of trapping, so the maximum M-deficit inversion is given as

$$M(z_{\rm top}) - M(0) - c_{\rm lap} z_{\rm top} > -60, \qquad (7)$$

where usually $c_{\rm lap} = 0.118$ M units/m.

Because the more the constraint conditions, the more correctly the problem may be described. Another meteorological constraint condition is used; the maximum M-deficit inversion is given as follows:

$$M(0) - M(z_{\rm top}) > 14. \qquad (8)$$

Equations (7) and (8) both could be likely to be derived from climatology.

5.2. Experiments result with meteorology constraints

Because the two parameters are strongly correlated for M deficits larger than about 60 M units, they are insensitive to the combination of thickness and M deficit. As shown in Fig. 4(b), the implementing of the constraint described in Subsection 5.1 reduces the search space so that only the smaller M deficit is allowed. This constraint will influence all inversion parameters, especially the M deficit and the mixed-layer slope.[19]

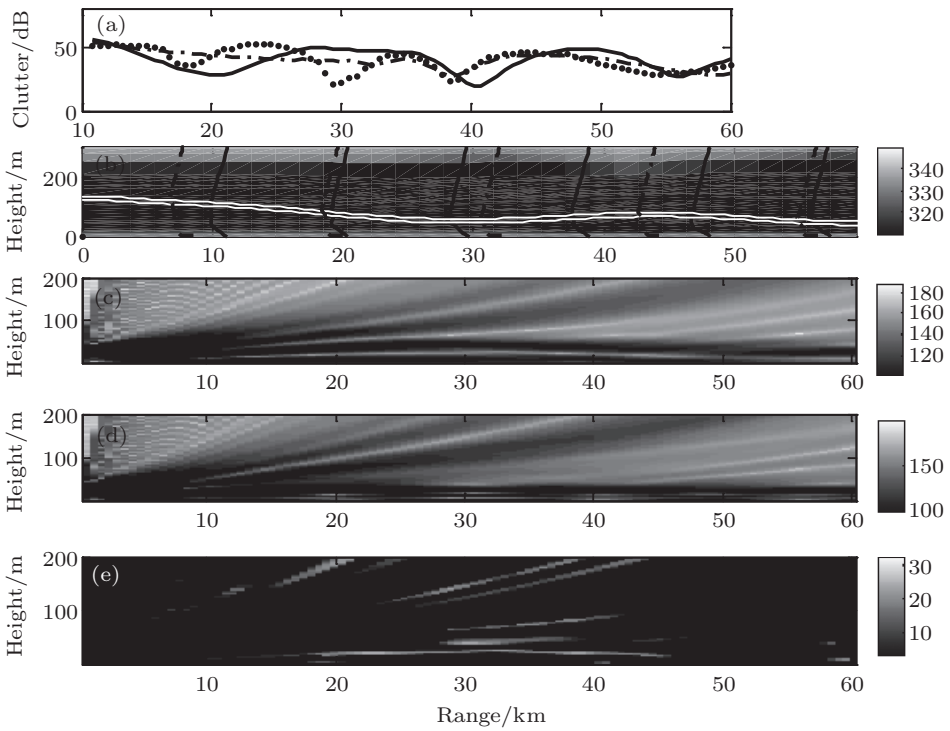


Fig. 4. Inversion based on the clutter return shown in Fig. 2 along azimuth 150° with meteorology constraints: (a) the clutter return (dB) as observed by the radar data (dotted), the modeled return using the retrieval profile (dash dotted) and modeled return from the observed profile (solid line); (b) observed profiles measured from helicopter (solid line) and inverted profiles (dash dotted); (c) coverage diagram (dB) corresponding to the inverted profiles; (d) coverage diagram (dB) based on helicopter profiles; (e) difference (dB) between coverage diagrams Figs. 4(c) and 4(d).

The result of the constrained inversion is shown in Figs 4(a) and 4(b). It is seen that the fitting to the clutter returns does not change the original results significantly (Fig. 4(a)). However, the retrieved profiles appear more reasonable (Fig. 4(b)). Furthermore, the difference between the propagation loss from the helicopter profiles and that from inverted profiles is quite low, even above the duct (Fig. 4(e)).

6. Conclusion

The principle of remote sensing of refractivity profile is described. Refractivity parameter inversion belongs to the field of inverse problems, which is severely ill-posed. A multi-parameter range-dependent parameterization is introduced and a genetic algorithm is employed to handle the large search space. It is shown that within the duct itself, the accuracy of the radar-inferred propagation-loss values approaches that of loss values calculated using a midpath sounding. This finding is based on an analysis that would tend to favour the midpath sounding. It is demonstrated that the inclusion of prior information alleviates this problem to a large degree.

The parameterization and the search bounds that are used could easily accommodate refractivity profiles found in other sea regions of the world. The advantage of this method is the nearly real time working, which makes RFC more attractive for operational use. Thus we have no reason to suspect that the performance of the algorithm will degrade when implemented observation data where the typical refractivity structures differ from the cases used here. In contrast to Figs. 4 and 3, the more the used meteorological constraint conditions, the more fitting results can be obtained. Therefore more complex environment and meteorological constraint conditions will be further explored in future work.

Acknowledgement

The authors would like to thank professor Gerstoft P and Yardim C, in Marine Physical Laboratory, University of California, San Diego, for providing SPANDAR data.

References

[1] Patterson W 1992 *Ducting Climatology Summary* (San Diego: SPAWAR Sys. Cent Press)

[2] Rogers L T, Hattan C P and Stapleton J K 2000 *Radio Sci.* **35** 955

[3] Gerstoft P, Gingras D F, Rogers L T and Hodgkiss W S 2000 I*EEE Trans. Antennas Propag.* **48** 345

[4] Gerstoft P, Rogers L T, Krolik J K and Hodgkiss W S 2003 *Radio Sci.* **38** 2640

[5] Barrios A 2004 *Radio Sci.* **39** 2930

[6] Gerstoft P, Hodgkiss W S, Rogers L T and Jablecki M 2004 *Radio Sci.* **39** 3077

[7] Yardim C, Gerstoft P and Hodgkiss W S 2006 *IEEE Trans. Antennas Propag.* **54** 1318

[8] Vasudevan S anderson H R, Kraut S, Gerstoft P, Rogers L T and Krolik J L 2007 *Radio Sci.* **42** 3423

[9] Yardim C, Gerstoft P and Hodgkiss W S 2007 *Radio Sci.* **42** 3561

[10] Yardim C, Gerstoft P and Hodgkiss W S 2008 *IEEE Antennas Propag.* **56** 1058

[11] Douvenot R, Fabbro V, Gerstoft P, Bourlier C and Saillard J 2008 *Radio Sci.* **43** 3842

[12] Yardim C, Gerstoft P and Hodgkiss W S 2009 *Radio Sci.* **44** 3897

[13] Sheng Z and Huang S X 2009 *Acta Phys. Sin.* **58** 4328 (in Chinese)

[14] Sheng Z, Huang S X and Zheng G D 2009 *Acta Phys. Sin.* **58** 4335 (in Chinese)

[15] Sheng Z, Huang S X and Zhao X F 2009 *Acta Phys. Sin.* **58** 6627 (in Chinese)

[16] Brown G S 1998 *IEEE Trans. Antennas Propag.* **46** 1

[17] Toporkov J V, Awadallah R S and Brown G S 1999 *J. Opt. Soc. Am.* **16** 176

[18] West J C 2000 *IEEE Trans. Geosci. Remote Sens.* **38** 1609

[19] Sheng Z, Huang S X and Chen L 2009 *Journal of PLA University of Science and Technology* **10** 200 (in Chinese)